Computers in Biology and Medicine 87 (2017) 46–56

Contents lists available at ScienceDirect

Computers in Biology and Medicine

journal homepage: www.elsevier.com/locate/compbiomed

Optimal design of nanowire field-effect troponin sensors

Amirreza Khodadadian [a, *], Kiarash Hosseini [c], Ali Manzour-ol-Ajdad [c], Marjan Hedayati [c], Reza Kalantarinejad [c], Clemens Heitzinger [a, b]

[a] Institute for Analysis and Scientific Computing, Vienna University of Technology (TU Wien), Wiedner Hauptstraße 8–10, 1040 Vienna, Austria
[b] School of Mathematical and Statistical Sciences, Arizona State University, Tempe, AZ 85287, USA
[c] Shezan Research and Innovation Centre, No. 25, Innovation 2 St., Pardis TechPark, Tehran, Iran

ARTICLE INFO

Keywords:
Silicon nanowire
Field-effect transistor
Biosensor
Sensor response
Limit of detection

ABSTRACT

We propose a design strategy for affinity-based biosensors using nanowires for sensing and measuring biomarker concentration in biological samples. Such sensors have been shown to have superior properties compared to conventional biosensors in terms of LOD (limit of detection), response time, cost, and size. However, there are several parameters affecting the performance of such devices that must be determined. In order to solve the design problem, we have developed a comprehensive model based on stochastic transport equations that makes it possible to optimize the sensing behavior.

1. Introduction

Cardiovascular diseases (CVDs) are the leading cause of morbidity and mortality for both men and women in developed and developing countries [1]. In the US in 2010, the overall rate of death attributable to CVD was 235.5 per 100 000 [2]. Additionally, each year cardiovascular diseases cause over 4.3 million deaths (48%) in Europe and over 2.0 million deaths (42%) in the European Union [3]. Acute myocardial infarction (AMI), also known as heart attack, occurs when the flow of blood to the heart is blocked, most often by a build-up of fat, cholesterol, and other substances, which form a plaque in the arteries that feed the heart (coronary arteries). The interrupted blood flow can damage or destroy part of the heart muscle.

Rapid and accurate diagnosis of CVDs is extremely important since it increases patient survival and saves enormous costs for the health-care system. An electrocardiogram (ECG) is a traditional test that checks for problems with the heart electrical activity. However, ECG is a poor diagnostic test for AMI, since more than half of the CVD patients who go to the Emergency Department show normal or no diagnostic electrocardiograms, which makes the early diagnosis of CVD more difficult [4,5]. A range of biochemical markers are available for diagnosis of AMI of which the cardiac troponins, namely cardiac troponin T (cTnT), and cardiac troponin I (cTnI), are the newest and clinically the most interesting. The unique features of the cardiac troponins (cTn) are that they are highly sensitive and specific for myocardial damage and they are prognostic [6,7]. In patients with suspected myocardial infarction or minor myocardial damage, cTn was found in their blood. However, in the many cases, creatine kinase-MB (CK-MB) mass was not increased and the ECGs did not indicate any cardiac problem [8,9]. Enzyme-linked immunosorbent assay (ELISA) [10] is one of the most popular techniques that may be used for cardiac biomarker detection since it ensures high diagnostic accuracy. However, the method has several drawbacks, such as long diagnostic time, which may range from hours to days due to laborious bio-analytical methodologies, or delay in the transportation of samples [11]. The method requires highly skilled laboratory staff and considerable investment in resources and equipment, and it is not often sensitive or fast enough for early diagnosis and treatment [12]. Furthermore, the technique is not able to allow for the label-free and highly targeted detection of sub 10 pg/mL concentrations of troponin [8,12].

Nowadays, several CVD marker detection sensors have been developed to overcome the disadvantages of ELISA. Surface plasma resonance (SPR) based biosensors [13], fluorescence-based sensors [14], and electrochemiluminescence-based biosensors [15] are a few of the biomarker detection methods. These methods require labeling, which leads to increased detection time and complexity of the sensor device [16]. Therefore, the development of accurate, inexpensive, fast response and high sensitive diagnostic device to detect cTn in blood is necessary. Silicon nanowire (SiNW) field-effect transistors (FETs) [17–19] have shown high sensitivity and a noticeable capability to detect specific biological species. They have received substantial interests because they are ultrasensitive, selective, low-cost devices and they can be fabricated using commercial microfabrication technology. The devices are designed

* Corresponding author.
E-mail address: Amirreza.Khodadadian@TUWien.ac.at (A. Khodadadian).

http://dx.doi.org/10.1016/j.compbiomed.2017.05.008
Received 11 February 2017; Received in revised form 9 May 2017; Accepted 9 May 2017

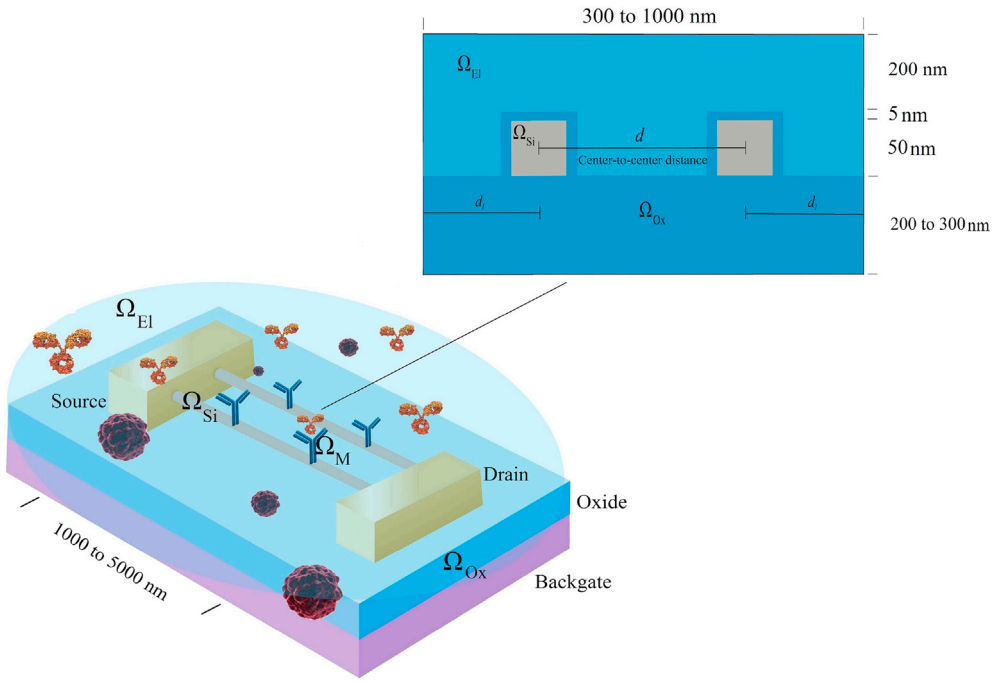

Fig. 1. Schematic diagram of the nanowire field-effect sensor showing receptor and target molecules. The subdomains, i.e., silicon nanowire Ω_{Si}, insulator Ω_{Ox}, the specific binding of target to probe molecules Ω_M, and the electrolyte Ω_{El} are illustrated with their dimensions and ranges. Additionally, d indicates the center-to-center distance between the nanowires and d_1 is the distance between a nanowire and the boundary.

to detect and quantify biological species, e.g., cancer cells [20], tumor-initiating cells [21], DNA/miRNA [22,23], and proteins [24]. Hence, SiNW-FETs are very promising candidates for the sensitive electrical detection of the biomarkers since they are reliable, label-free, and rapid response and they are able to detect subpicomolar concentrations of target species [12].

The specificity of the biosensor system is given by the immobilized biomolecules. In fact, the devices are fabricated by immobilizing biological receptor materials (in this case the antibodies [12]) on the surface of a suitable transducer that converts the biochemical signal into a quantifiable electronic signal [25]. Proteins are charged in the electrolyte (in our case blood) and can be detected by the sensors when the suitable receptors are linked to the nanowire surface [19]. As target molecules (here cTn) bind to the immobilized probe molecules on the surface layer, the charge distribution changes and modulates the conductance of the semiconductor transducer, similarly to the effect that a change in gate voltage has on a MOSFET. In other words, the changes of the device conductivity is the response of the sensor to the specific binding of cardiac troponins to the anti-troponin probes [12] on the surface.

In Ref. [12], a CMOS compatible method to fabricate an array of highly ordered SiNW for detection of very low concentrations of cTn was presented. This work indicates that the changes in conductance of the device provide a label-free detection method of biomarkers which eliminates the necessity of expensive and complicated diagnostic tools. The advantages of affinity-based biosensors such as high sensitivity and reliable detection of cardiac markers including cTnT and cTnI, myoglobin, etc., were shown in Ref. [25] in detail. The changes of the electrical characteristics of SiNW-FETs such as drain current and sensitivity due to the specific binding were explained in Ref. [16].

The purpose of the present work is the development and quantitative understanding of biological sensors for the detection of cardiac troponin in blood starting just from its known structure (PDB code 1MXL [26]). We determine the effective parameters to design and fabricate more sensitive nanowire field-effect sensors to detect different ranges of cTn. Here, the sensitivity indicates the response of the sensor to the binding of target molecules (cTn) to the immobilized probe molecules (anti-troponin receptors) at the sensor surface.

As for every sensor, a crucial question is how to achieve the best response of the SiNW-FET. There are several substantial parameters which are effective in the conductivity of the device. In other words, the sensor response is influenced by different physical and geometric device properties. In this work, we propose an array of silicon-nanowire field-effect biosensors optimized with regard to parameters such as length, width, doping concentration, dopant type, type of the nanowire, backgate voltage, and the number of parallel nanowires. Thus, by changing influential parameters, it is made possible to optimize the electrical characteristics of devices and to fabricate the optimal field-effect sensor to detect cTn concentration more accurately. Noise and fluctuations of the device conductivity due to the random binding of cTn to the receptors are also taken into account. Therefore, we introduce a comprehensive physical/mathematical model based on partial differential equations (PDEs) in order to model the electrical characteristics of SiNW-FETs.

The rest of the paper is organized as follows. In Section 2.1, we present the cardiac troponin sensitive sensor and explain its physical characteristics. Also, we describe a PDE based model to study the sensor electrical behavior. In Section 3, we present numerical results to study the physical behavior of the nanowire sensors by varying the parameters. Influential parameters in order to the intensify the sensor response to cTn are discussed. Finally, the conclusions are drawn in Section 4.

2. Modeling of cardiac troponin sensors

The troponin complex regulates the contraction of striated muscles. It consists of three subunits, i.e., cTnC, cTnT, and cTnI. These protein subunits along with tropomyosin are located on the actin filament and are essential for the calcium-mediated regulation of skeletal and cardiac muscle contraction [27]. Cardiac TnT binds the troponin components to tropomyosin and TnI inhibits the interaction of myosin with actin [28,29]. Cardiac TnC contains the binding sites for Ca^{2+} and its interaction with cTnI and cTnT is central to the regulation of skeletal and cardiac muscle contraction [30]. TnT and TnI have been found to have excellent sensitivity and specificity, and are superior to CK-MB as indicators of myocardial necrosis [31]. For the last twenty-five years, isoforms of troponin I and T have been widely used for immunochemical

diagnostics of pathologies associated with cardiomyocyte death, e.g. AMI, unstable angina, post-surgery myocardial trauma, and other diseases related to cardiac muscle injury [32].

Cardiac TnI and TnT are released after AMI or other cardiacs disease [28] and their clinical sensitivity and specificity improve with time. More precisely, for both troponins, sensitivity raises from 10% to 45% within 1 h of the onset of pain to more than 90% after 8 or more hours [33]. Specificity does not change noticeably over time. It decreases from 87% to 80% from 1 to 12 h after the onset of chest pain for troponin T and is approximately 95% for troponin I [33]. The diagnostic performance/accuracy of TnI and TnT has been observed similarly and is very high [7].

Few studies have reported the 99th percentile of high-sensitive cardiac troponin I (hscTnI) among different age groups and genders. Since 1995, the diagnostic cutoff has been decreased from 1500 pg/mL to 10 pg/mL [34,35]. As in Ref. [35], the 99th percentile concentration of TnI was greater than 19 pg/mL for individuals older than 60 years and 10 pg/mL for individuals younger than 60 years. Therefore, concentrations greater than 10 pg/mL have been shown to have prognostic value. In other words, the upper limit for a normal individual is 10 pg/mL, and for patients who have acute coronary syndromes or AMI, rising troponin values greater than or equal to the diagnostic cutoff value result in the diagnosis of cardiac injury. Also, decreasing values are indicative of recent cardiac injury. We also consider that patients with low-level elevations (smaller than 20 pg/mL) of TnI and diagnostic uncertainty for acute coronary syndrome should be evaluated by repeated measurements.

Over the last fifteen years, new techniques and strategies for rapid detection of biomarkers, including cardiac troponin, have been utilized to shorten the diagnostic time and increase the reliability of tests [19]. Quick determination of the concentration of biomarkers in the body has drawn attention in the past decade. New techniques are being incorporated into products [25]. As the medical diagnostic methods progress, therapies with high specificity according to biomarkers determined in tests are continuously being targeted. High-throughput sensors and systems for the ultrasensitive detection of biomolecular interactions are in high demand [16].

Here the main aim of the SiNW-FET is the detection of cardiac troponin in blood. For this reason, the sensor must be able to determine the target protein concentration in the meaningful range. In other words, the dynamic range of the sensor is to designed. The range of cardiac troponin in human blood is between 3.4 pg/mL and 10 000 pg/mL as the concentration rises from almost 20 pg/mL within one hour of myocardial infarction to 10 000 pg/mL after 32 h from the incidence [34,36].

The basic structure of the device including its dimensions is shown in Fig. 1. The domain Ω is partitioned into four subdomains with different physical properties. The silicon nanowire Ω_{Si} acts as the transducer of the sensor. The nanowire transducer is located on top of a dielectric material and covered by a second dielectric material Ω_{Ox}. The native oxide coating on the SiNW surface is an effective passivation layer which can be functionalized by cardiac troponin Ω_{M}. Finally, the target molecules are located in the electrolyte Ω_{El}.

Here, we consider four shapes or types of nanowires: rectangular, trapezoidal, radial, and triangular, all with a cross-sectional area of 2500 nm^2, a doping concentration ($\mathrm{C_{dop}}$) of 10^{17} cm^{-3}, protected by a 5 nm thick silicon oxide (Ω_{Ox}), and a thermal voltage of 26 mV. The applied voltages are $V_G = 1$ V at the back-gate contact and $V_{SD} = 0.2$ V as the source-to-drain voltage.

2.1. The stochastic transport equations

In the nanowire field-effect biosensor, the adsorption of biomolecules (cTn) on the SiNW results in a sufficient change of conductance for detection due to the field-effect [37]. In fact, as target molecules in the liquid bind to the receptors, their presence and their partial charges change the charge concentration in the boundary layer, which in turn modulates the conductance of the nanowire transducer. The most common and well-established continuum model for the description of ionic concentrations and the electrostatic interactions of the biomolecules is the Poisson-Boltzmann equation [38]. It can be used to calculate ionic concentrations around molecules and the effect of the charged target molecules (cTn) on the transducer.

In such biosensors, there are several sources of noise which must be taken into account. First, the random association of cTn to the receptors at the surface and their dissociation gives rise to noticeable noise [39–41]. Second, the positions of the probe molecules, as well as their orientations and the orientations of the probe-target complexes are random [39]. Since this type of noise is due to the biological interactions between target and probe molecules, it is called biological noise. Here, we use a comprehensive model of the devices that provides a physical and quantitative understanding of them. It is based on a system of PDEs coupled to a stochastic reaction model for the association/dissociation process. Also, it has been extended to a system of stochastic partial differential equations (SPDEs) in order make it possible to include noise and fluctuations. The details and the advantages of the model are discussed in Refs. [42–45]. The model consists of the Poisson-Boltzmann equation to model the electrolyte, the drift-diffusion-Poisson system to model the charge transport in the transducer, and a reaction equation to model the association of target molecules to the sensor surface and their dissociation. The model enables us to calculate the response of the sensor to cTn and estimate its variation due to the biological noise.

The model equation for the electrostatic potential in different subdomains is the Poisson–Boltzmann equation

$$-\nabla\cdot(A(x,\omega)\nabla V(x,\omega)) = \begin{cases} q\big(\mathrm{C_{dop}}(x,\omega) + p(x,\omega) - n(x,\omega)\big) & \text{in } \Omega_{\mathrm{Si}},\\ 0 & \text{in } \Omega_{\mathrm{Ox}},\\ \rho(x,\omega) & \text{in } \Omega_{\mathrm{M}},\\ -2\varphi\,\sinh(\beta(V(x,\omega) - \Phi_F(x,\omega))) & \text{in } \Omega_{\mathrm{El}}, \end{cases} \tag{1a}$$

where $\boldsymbol{x} \in \Omega$, $\boldsymbol{\omega} = (\omega_1, \ldots, \omega_n)$ is an element of the probability space, and V is the electrostatic potential. The dielectric constants for silicon nanowire, oxide layer, probe-target molecules, and the electrolyte are $A_{\mathrm{Si}} = 11.7A_0$, $A_{\mathrm{Ox}} = 3.9A_0$, $A_{\mathrm{M}} = 3.7A_0$, and $A_{\mathrm{El}} = 78A_0$, respectively, where $A_0 = 8.85 \times 10^{-12}$ F/m. In the electrolyte, φ indicates the ionic bulk concentration. In Ω_{M}, the fixed charge concentration ρ is the charge of the probe-target molecules (see Section 2.3). Also, in the transducer Ω_{Si}, $\mathrm{C_{dop}}$ is the doping concentration.

The concentration $p(x, \omega)$ of positive free charge carriers and the concentration $n(x, \omega)$ of negative ones are given by Boltzmann distributions as

$$p(x,\omega) = n_i \exp\left(-\frac{q(V(x,\omega) - \Phi_F)}{k_B T}\right), \tag{2a}$$

$$n(x,\omega) = n_i \exp\left(\frac{q(V(x,\omega) - \Phi_F)}{k_B T}\right). \tag{2b}$$

Here, q is the elementary charge, $\beta := q/(k_B T)$, where k_B is the Boltzmann constant, T is the temperature, Φ_F is the Fermi level, and $n_i = 1.5 \times 10^{10}$ cm^{-3} is the intrinsic carrier concentration. Additionally, homogenization of an elliptic problem with a periodic boundary layer at a manifold Γ yields the two interface conditions [46].

$$V(0+, y, \omega) - V(0-, y, \omega) = \alpha(y, \omega),$$
$$A(0+)\partial_x V(0+, y, \omega) - A(0-)\partial_x V(0-, y, \omega) = \gamma(y, \omega)$$

between the semiconductor and the liquid. Here $0+$ denotes the limit at the interface on the side of the liquid, while $0-$ is the limit on the side of the silicon-oxide layer. Here, for the sake of notational simplicity, we denote the one-dimensional coordinate orthogonal to Γ by x and the remaining $(d-1)$-dimensional coordinates by y. The oscillating charge

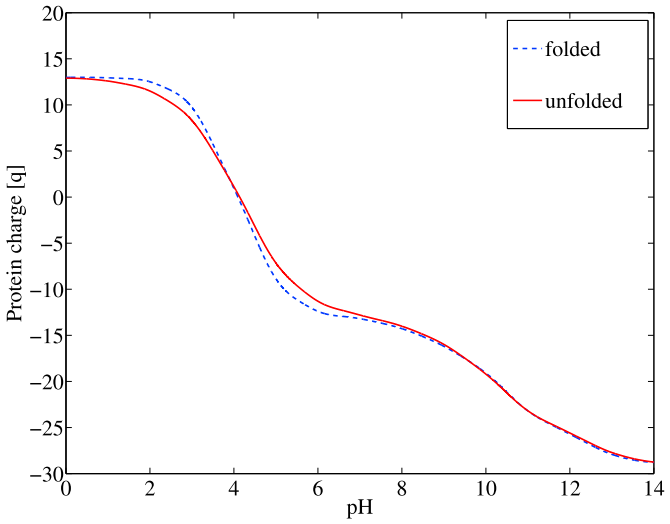

Fig. 2. The net charge of the folded and unfolded states of protein 1MXL for different pH values. The results are obtained by PDB2PQR simulation.

concentration in the surface layer is described by the macroscopic dipole moment density α and the macroscopic surface charge density γ after homogenization.

As mentioned above, the electrical conductance change is the sensor response to specific binding of the biomolecules to the functionalized surface in label-free detection. In other words, monitoring changes in conductance of the SiNW-FET device is used to detect the different concentrations of troponin. In the semiconducting part Ω_{Si} of the device, the drift-diffusion-Poisson system

$$-\nabla\cdot(A\nabla V) = q\big(C_{\text{dop}} + p - n\big), \tag{3a}$$

$$\nabla\cdot J_n = -qR, \tag{3b}$$

$$\nabla\cdot J_p = qR, \tag{3c}$$

$$J_n = q(D_n\nabla n - \mu_n n\nabla V), \tag{3d}$$

$$J_p = q\big(-D_p\nabla p - \mu_p p\nabla V\big) \tag{3e}$$

is used to model charge transport. Here, J_n and J_p are the current densities, μ_n and μ_p are the electron and hole mobilities, and $D_n := U_T\mu_n$ and $D_p := U_T\mu_p$ are the diffusion coefficients with $U_T := k_BT/q$ as the thermal voltage. Also, we use the Shockley-Read-Hall recombination rate R, which is defined by

$$R(n,p) := \frac{np - n_i^2}{\tau_n(p+n_i) + \tau_p(n+n_i)},$$

where τ_n and τ_p are the lifetimes of the free carriers. The electrical current is obtained by the integration of the current density over a cross section of the nanowire. Finally, the details of solving the system of equations with the lowest computational complexity are given in Ref. [42].

2.2. The stochastic surface reactions

As target molecules (cTn) bind to receptor molecules (anti-troponin probes), the charge concentration of the boundary layer is changed and therefore the current through the semiconducting nanowire is modulated. The association and dissociation processes of target molecules to the receptors at the surface are described by the reaction equations

$$\mathbf{T} + \mathbf{P} \overset{r_a}{\rightleftarrows} \mathbf{PT}, \tag{4a}$$

$$\mathbf{PT} \overset{r_d}{\rightleftarrows} \mathbf{P} + \mathbf{T}. \tag{4b}$$

Here, **T** denotes the target molecules, **P** denotes the receptor molecule, **PT** denotes a probe-target complex at the sensor surface and r_a and r_d are the reaction constants of the association and dissociation processes, respectively. Due to the relatively small number of molecules (i.e., few bound cardiac troponins to the antibodies) present at the sensor surface, their association and dissociation are modeled as a stochastic process yielding the Langevin equation [40].

$$\mathrm{d}\mathbf{PT}_t = (r_a\mathbf{T}(\mathbf{P} - \mathbf{PT_t}) - r_d\mathbf{PT})\mathrm{d}t + \sqrt{r_a\mathbf{T}(\mathbf{P} - \mathbf{PT}_t)}\mathrm{d}B_1 - \sqrt{r_d\mathbf{PT}_t}\mathrm{d}B_2, \tag{5a}$$

$$\mathbf{PT}_0 = 0, \tag{5b}$$

where the $\mathrm{d}B_i$ indicate Wiener processes. The initial condition corresponds to no probe-target complex being present at the surface in the beginning. The calculation of the expected value, variance, and the binding efficiency with respect to different target molecule concentrations can be found in Ref. [40].

2.3. The charge of biomolecules

The modeling of the electrostatics of biomolecules is essential for the simulation of nanowire field-effect sensors. The surface of dielectric materials such as SiO_2, Si_3N_4, Al_2O_3, and Ta_2O_5 is charged when it is in contact with an electrolyte and it is neutral only at the isoelectric point. This surface charge provides an important baseline value regarding the operating regime of the sensor since the surface charge is a function of pH value [47]. There are several methods to describe the effect of charged molecules: the atomistic approach, i.e., Monte-Carlo simulations [48], the continuum approach, i.e., the Poisson-Boltzmann equation [38,49], and the empirical PROPKA model [50].

The pK_a values of the ionizable residues are the negative logarithm of the ratio of dissociated acid and conjugated base over the concentration of the associated chemical. They are the basis for understanding the pH-dependent characteristics of proteins and catalytic mechanisms of many enzymes. Here, the program PDB2PQR [51] is used to compute the charge distributions of proteins of known structure. Given a protein structure, it computes the pK_a value of each ionizable amino acid. Based on the computed pK_a value, it is possible to determine the protonation state of each ionizable amino acid based on pH value [51].

Fig. 2 shows the troponin (PDB code 1MXL) charge of the folded and unfolded states as a function of pH values between 0 and 14. Here the folded molecule carries no net electrical charge at a pH value of 4.13, while for unfolded proteins the isoelectric point is a pH value of 4.08. Blood is normally slightly basic in a pH range of 7.35–7.45. According to the simulation, the protein total charge is − 13.58 q at blood pH (7.4 in this work). The net charges of the target molecules are negative since the protein isoelectric values are lower than pH 7.4. Finally, the negative charges of the target protein (cTn) result in a carrier accumulation on the silicon nanowire and consequently an increase of conductance.

2.4. Sensor response (sensitivity)

In field-effect biosensors, the target molecules (cTn) carry negative (due to blood pH value) charges and act as a negative gate voltage. Since we use a P-type (boron-doped) semiconductor as the transducer, the accumulation of charge carriers increases the conductance as well. The critical issue for the modeling of the sensitivity of nanowire field-effect sensors is the screening of the partial charges of the target molecules by the free ions.

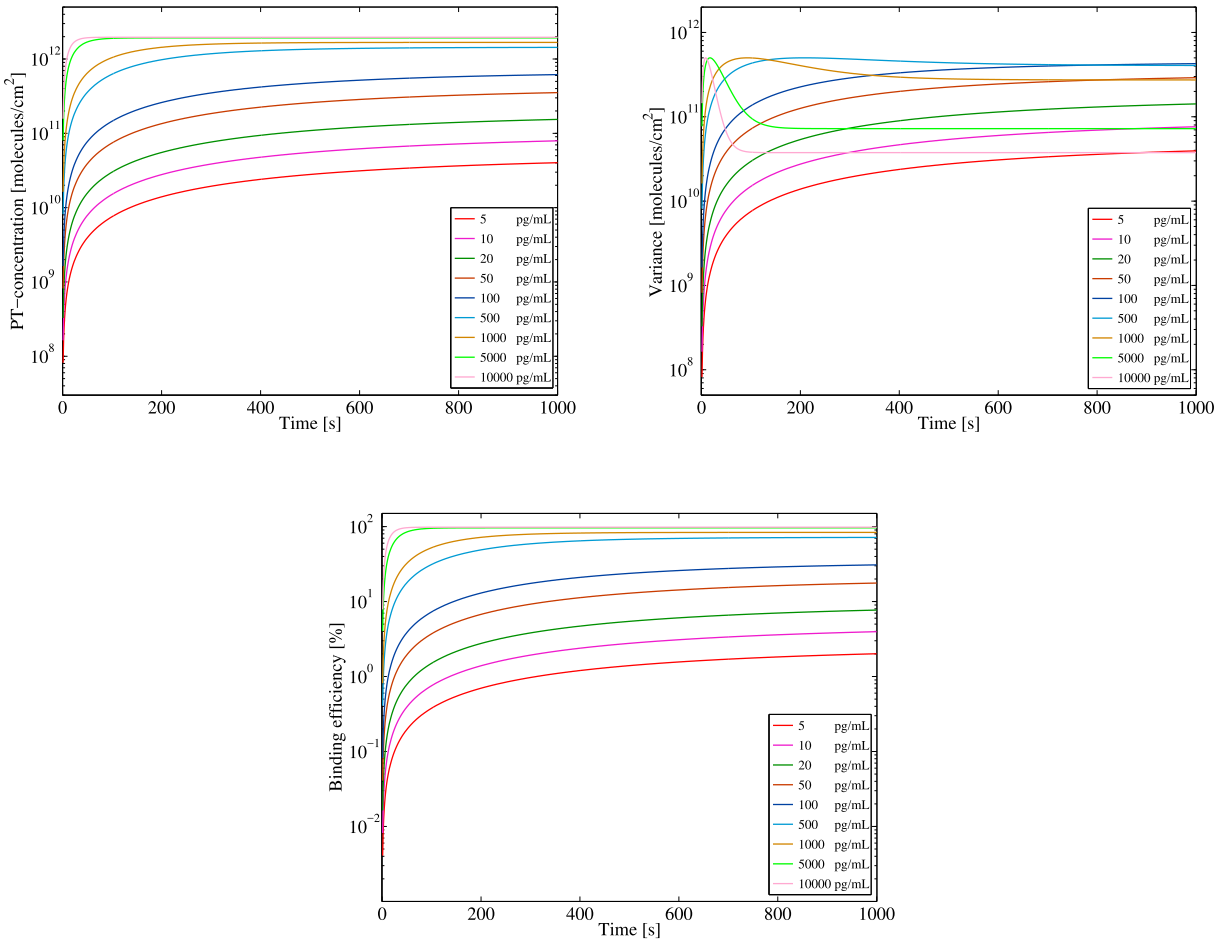

Fig. 3. The expected value (top left), variance (top right), and binding efficiency (bottom) of **PT**-complexes for different troponin concentrations.

Definition 1. *The sensor response (sensitivity) is defined as*

$$\frac{I_{mol} - I_0}{I_0}, \tag{6}$$

where I_{mol} and I_0 are the currents through the device with and without molecules, respectively.

In the subsequent simulations, we consider I_{mol} as the signal. This quantity can be interpreted as the response of the sensor to the specific binding of cTn to the anti-troponin receptors.

2.5. The signal-to-noise ratio

As explained in 2.2, due to the random association/dissociation process, the number of target molecules bound to probe molecules is a random process.

Definition 2. (Signal-to-noise ratio). *The signal-to-noise ratio (SNR) is defined as*

$$\mathrm{SNR}(I) := \frac{\mathbb{E}(I_{\mathrm{mol}})}{\sigma(I_{\mathrm{mol}})},$$

where σ denotes the standard deviation.

2.6. Limit of detection

The limit of detection (LOD) of an individual analytical procedure is the lowest amount of analyte in a sample which can be detected, but not necessarily quantified. In field-effect sensors, surface reactions at the oxide surface depending on the pH value and the binding of charged target molecules result in changes in the charge concentration at and near the surface, and subsequently in changes in the electrostatic potential, which then modulate the current through the transducer. Here, the LOD is defined as the minimum troponin concentration that induces a measurable difference in output current. A signal-to-noise ratio larger than 5 is generally considered acceptable for determining the detection limit.

3. Numerical results

By solving the system of model equations in Section 2.1, the current-voltage characteristics and the sensor response are determined as functions of the target molecule concentration. Hence the behavior of the nanowire sensors can be studied by varying all influential device parameters.

First, we calculate the statistics of the **PT**-complex by solving the Langevin equation. As mentioned already, the dynamic TnI range is between 3.4 pg/mL and 10 000 pg/mL. To convert the troponin concentration to a number of molecules, the protein weight of 24 000 Da is used. In the simulations, we also used $C_P := 2 \times 10^{12}$ cm^{-2} as the probe density, and the association and dissociation constants $r_a = 3933$ and $r_d = 0.0016$ are taken from Refs. [40,52].

Fig. 3 shows the results of the simulation for different concentrations of target molecules. For the lower concentrations (less than 10 pg/mL), the ratio of hybridized complexes at the surface to the total number of probe molecules is less than 10%. In this range, the equilibrium time is also considerably larger than for higher concentrations. On the other

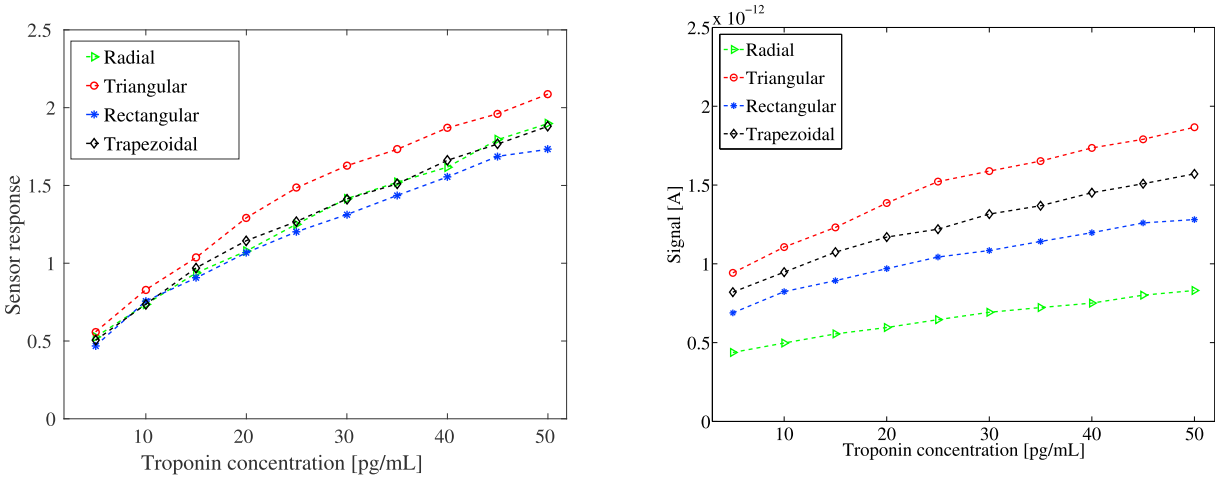

Fig. 4. Sensor response (left) and signal (right) as a function of troponin concentration varying from 5 pg/ml and 50 pg/ml for different nanowire cross sections. The sensors are 300 nm wide and the bulk oxide is 200 nm thick. Each sensor has one 1000 nm long nanowire, a cross-sectional area of 2500 nm^2, a doping concentration of 10^{17} cm^{-3}, and they are protected by a 5 nm thick silicon oxide layer.

hand, for concentrations higher than 500 pg/mL, the binding efficiency attains a very good value of nearly 100% and the equilibrium time is less than 200 s. Moreover, a remarkable feature of such a field-effect sensors is that even if the binding efficiency is low for certain probe and target concentrations, the surface charge density can be larger and therefore result in better detection by a field-effect sensor. Finally, for all troponin concentrations, the binding time (of cTn to the antibodies) shows the very fast response of the sensor. This reaction time indicates the significance of using SiNW-FETs compared to traditional methods such as ELISA.

Using the 99th percentile among different age groups and genders, cTnI assay values are more than 19 pg/mL in individuals older than 60 years and 10 pg/mL in the rest of the individuals [53]. A sharp increase in the troponin concentration is observed after two to three hours after the onset of symptoms, e.g., chest pain. For example, in Ref. [34], the value raised from 60 pg/mL to 6.3 ng/mL six hours after the medical examination.

According to these concentrations mentioned in the literature, we define three different concentration ranges and design three sensors, one for each concentration range.

For the first concentration range (low risk or healthy patients), the device is designed for a concentration between 5 pg/mL and 50 pg/mL. The sensor is 300 nm wide and is characterized by a 200 nm thick bulk oxide; the length of the nanowire is 1000 nm.

In acute coronary syndrome, the concentration reaches 500 pg/mL after three hours [34]. Therefore, the second concentration range is defined to be 50 pg/mL to 500 pg/mL. Here, the width of this device is 1 μm, the length of the nanowire is 5 μm, and the height of the bulk oxide and the substrate is 300 nm. To consider the situation when many molecules may bind, two parallel nanowires are used.

The cTnI value rises to its peak value of 10 ng/mL within twenty hours and then it decreases gradually [34]. The third and highest concentration range is thus from 500 pg/mL to 10 ng/mL. For this range, the sensor is an array of four nanowires for improved detection of high concentrations.

The first comparison discusses the effect of the four different cross sections of nanowires in the first device. Fig. 4 shows the results for the first device, the one for healthy or low-risk concentration, for different cross sections, all with a cross-sectional area of 2500 nm^2 and a length of 1000 nm.

The figure shows that the triangular nanowire performs considerably better than the other transducers, especially for concentrations higher than 10 pg/mL. The radial and trapezoidal nanowires show approximately the same sensor response for most of the concentrations and perform better than the rectangular shape. However, the sensitivity of the rectangular transducer at the diagnostic cutoff is slightly better than the

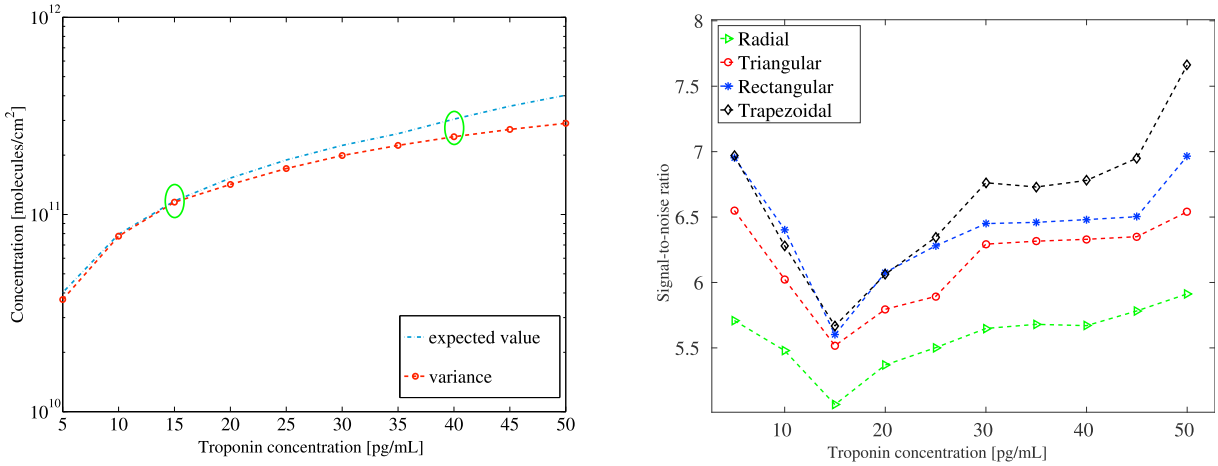

Fig. 5. Expected value and variance of **PT**-complexes (left) and signal-to-noise ratio (right) as a function of troponin concentration varying from 5 pg/ml and 50 pg/ml for different nanowire cross sections. The sensors are 300 nm wide and the bulk oxide is 200 nm thick. Each sensor has one 1000 nm long nanowire, a cross-sectional area of 2500 nm^2, a doping concentration of 10^{17} cm^{-3}, and they are protected by a 5 nm thick silicon oxide layer.

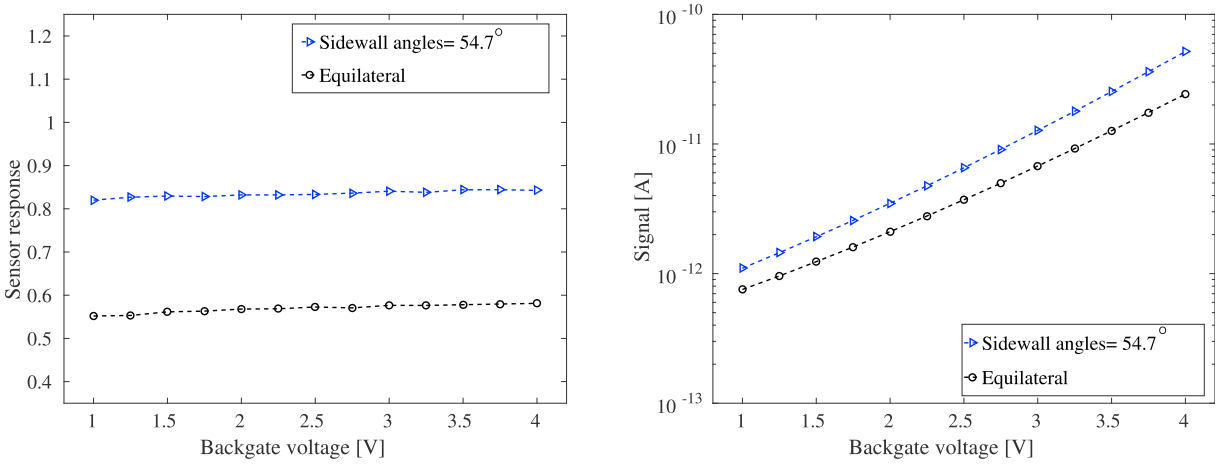

Fig. 6. Sensor response (left) and signal (right) of two triangular nanowires for different backgate voltages at 10 pg/mL troponin concentration. The sensors are 300 nm wide and the bulk oxide is 200 nm thick. Each sensor has one 1000 nm long nanowire, a cross-sectional area of 2500 nm^2, a doping concentration of 10^{17} cm^{-3}, and they are protected by a 5 nm thick silicon oxide layer.

trapezoidal and radial ones.

The radial nanowire yields the lowest signal compared to the others, while the triangular cross section again yields the highest current. As already mentioned, the device conductivity depends on the density of bound analytes. Fig. 5 illustrates the variation in the number of probe-target complexes for cTn concentration between 5 pg/mL and 50 pg/mL. The results indicate that from 5 pg/mL to 15 pg/mL the variance increases sharper than the expected value. As a consequence, as shown in Fig. 5, for this range the SNR is sloped downward since the current variance is sloped upward. For higher concentrations, more **PT**-complexes increase the signal, which counteracts the increase in noise. Therefore, in all sensors, the SNR shows a gradual upward trend. Furthermore, in spite of the fact that the triangular nanowire yields a higher signal, the higher noise in this device compared to the rectangular

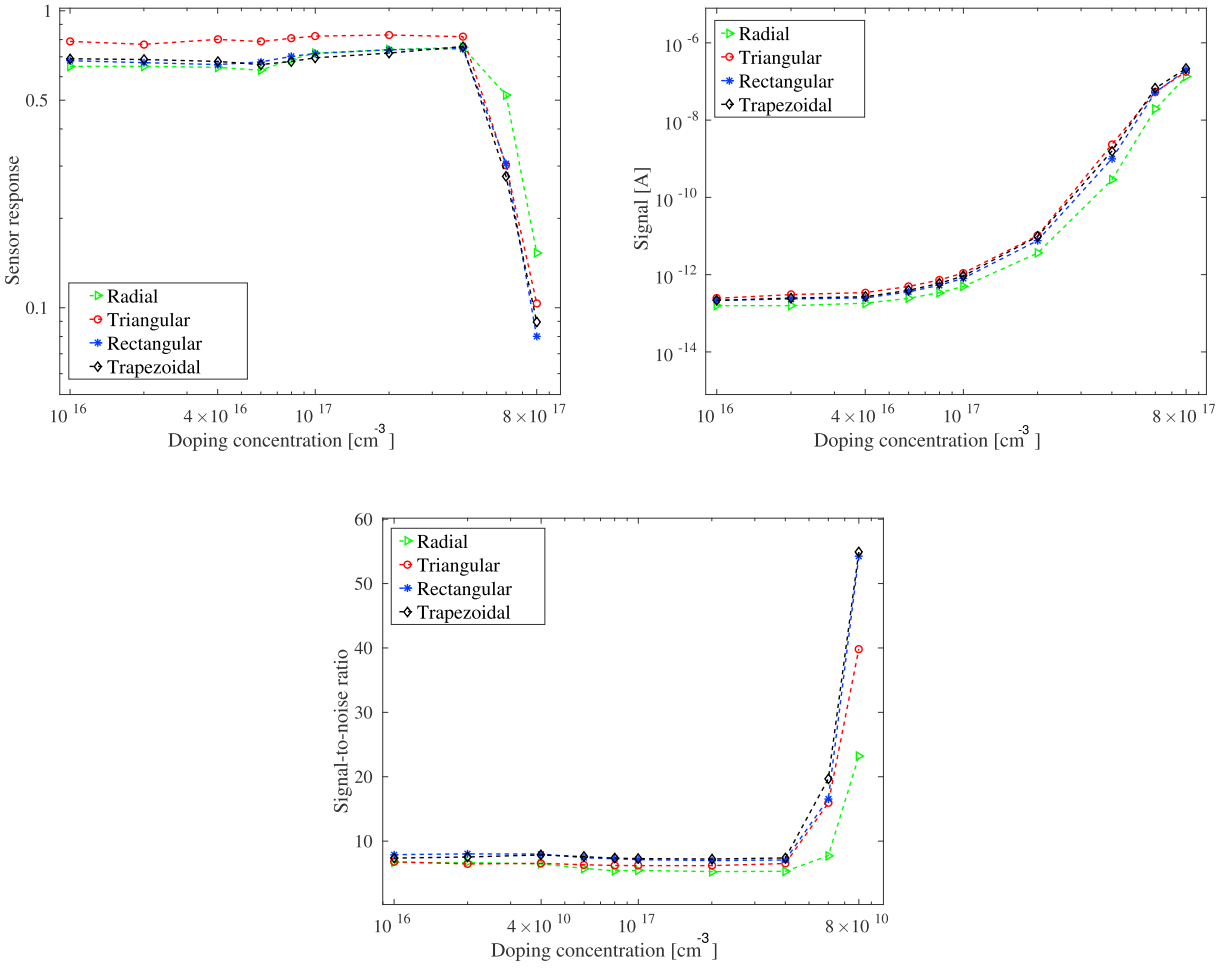

Fig. 7. Sensor response (top left), signal (top right), and SNR (bottom) as a function of doping concentration for different nanowire cross sections. The sensors are 300 nm wide and the bulk oxide is 200 nm thick. Each sensor has one 1000 nm long nanowire, a cross-sectional area of 2500 nm^2 and they are protected by a 5 nm thick silicon oxide layer.

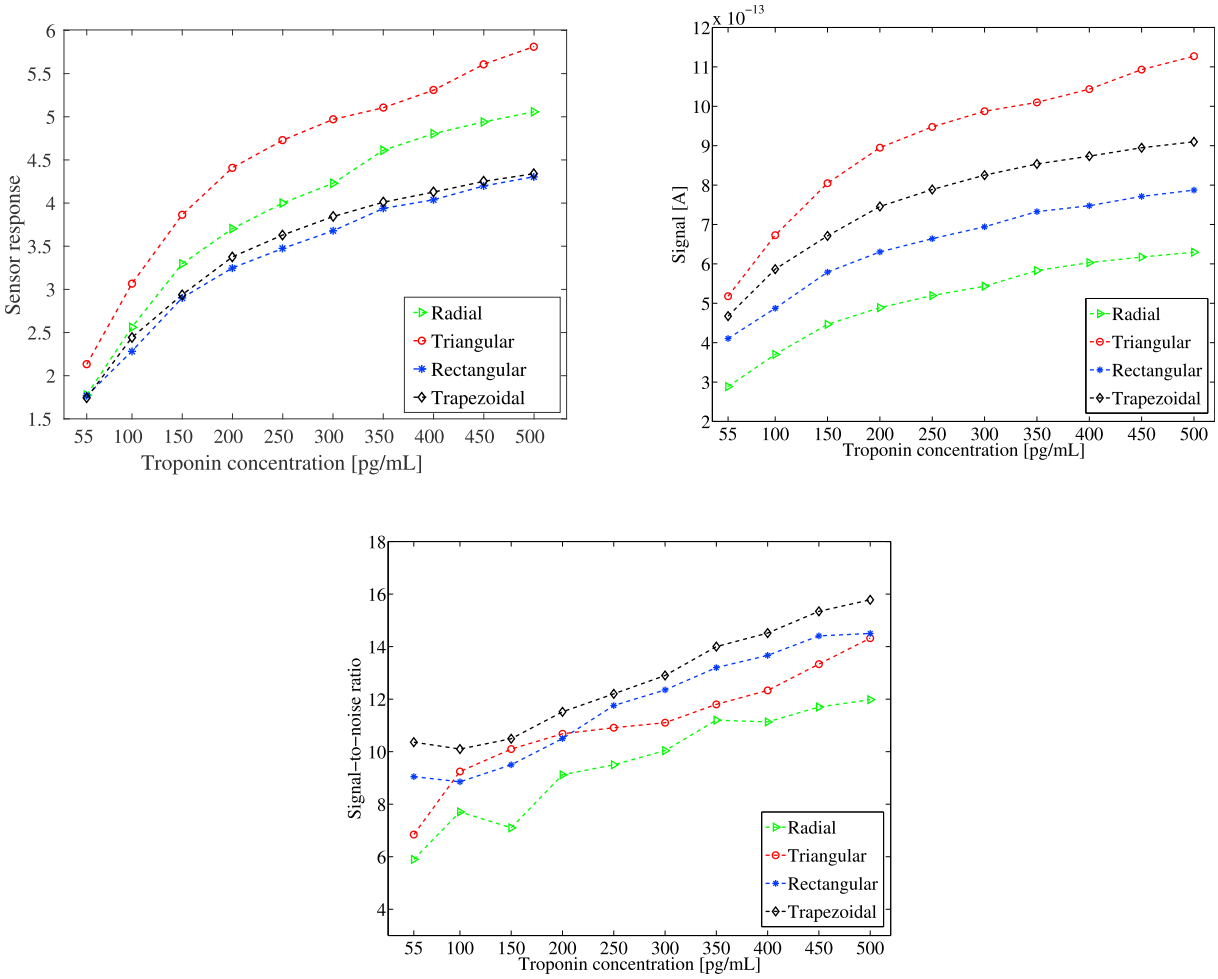

Fig. 8. Sensor response (top left), signal (top right), and SNR (bottom) as a function of troponin concentration varying from 5 pg/ml and 50 pg/ml for different nanowire cross sections. The sensors are 1000 nm wide and the bulk oxide is 300 nm thick. Each sensor has two parallel 5000 nm long nanowires, a cross-sectional area of 2500 nm^2, a doping concentration of 10^{17} cm^{-3}, and they are protected by a 5 nm thick silicon oxide layer.

and trapezoidal devices decreases the ratio. Again, due to a lower signal, the SNR for the radial nanowire is significantly lower than the rest of the devices. For more than 40 pg/mL, the **PT**-complex increase is pronounced compared to the variance. Therefore, as an inflection point, again the SNR shows an upward trend for the higher concentrations. Finally, we should note that the variation in the density of bound analytes leads to threshold voltage fluctuations since the threshold voltage variation depends only on the number of absorbed molecules [54,55].

A higher sensor response of SiNW-FETs depends considerably on the size of the device [56]. In Refs. [57,58], SiNW-FETs were fabricated by using commercially available (100) silicon-on-insulator wafers and anisotropic tetramethylammonium hydroxide (TMAH). Thus, a smooth triangular SiNW-FET is produced with a sidewall angle of ≈54.7° to the horizontal surface and (111) silicon sidewall plane. In Fig. 6, the sensor response for the mentioned triangular device and for an equilateral cross section are given. The figure shows the sensitivity and the signal for both triangular cross sections as functions of different backgate voltages. The performance of the (111) planes compared to the equilateral transducer is noticeably better. Concerning the voltage, the figure shows that the sensitivity is not considerably affected by the gate voltage, although a slight increase is observed. On the other hand, the signal in both devices rise noticeably as the backgate voltage increases.

The optimal doping concentration is a crucial design parameter. Fig. 7 shows the effect of the doping concentration varying between 1×10^{16} cm^{-3} and 8×10^{17} cm^{-3}. According to the simulation results, although the sensor response shows a small fluctuation from $1 \times$

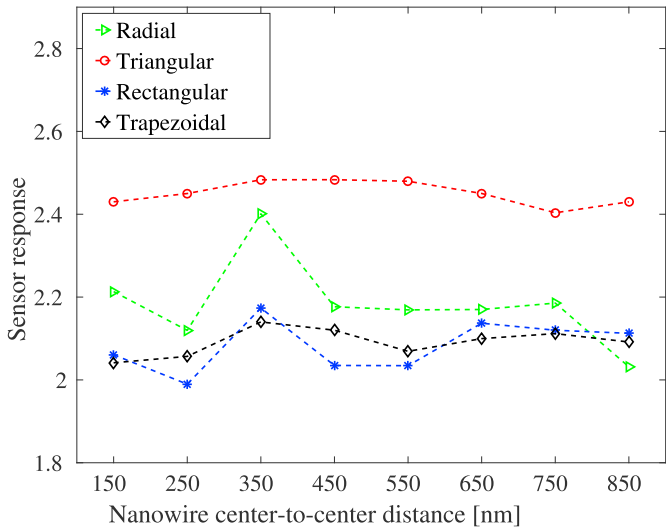

Fig. 9. The sensor response of different devices as a function of the nanowire center-to-center distance at 75 pg/ml cTn concentration. The sensors are 1000 nm wide and the bulk oxide is 300 nm thick. Each sensor has two parallel 5000 nm long nanowires, a cross-sectional area of 2500 nm^2, a doping concentration of 10^{17} cm^{-3}, and they are protected by a 5 nm thick silicon oxide layer.

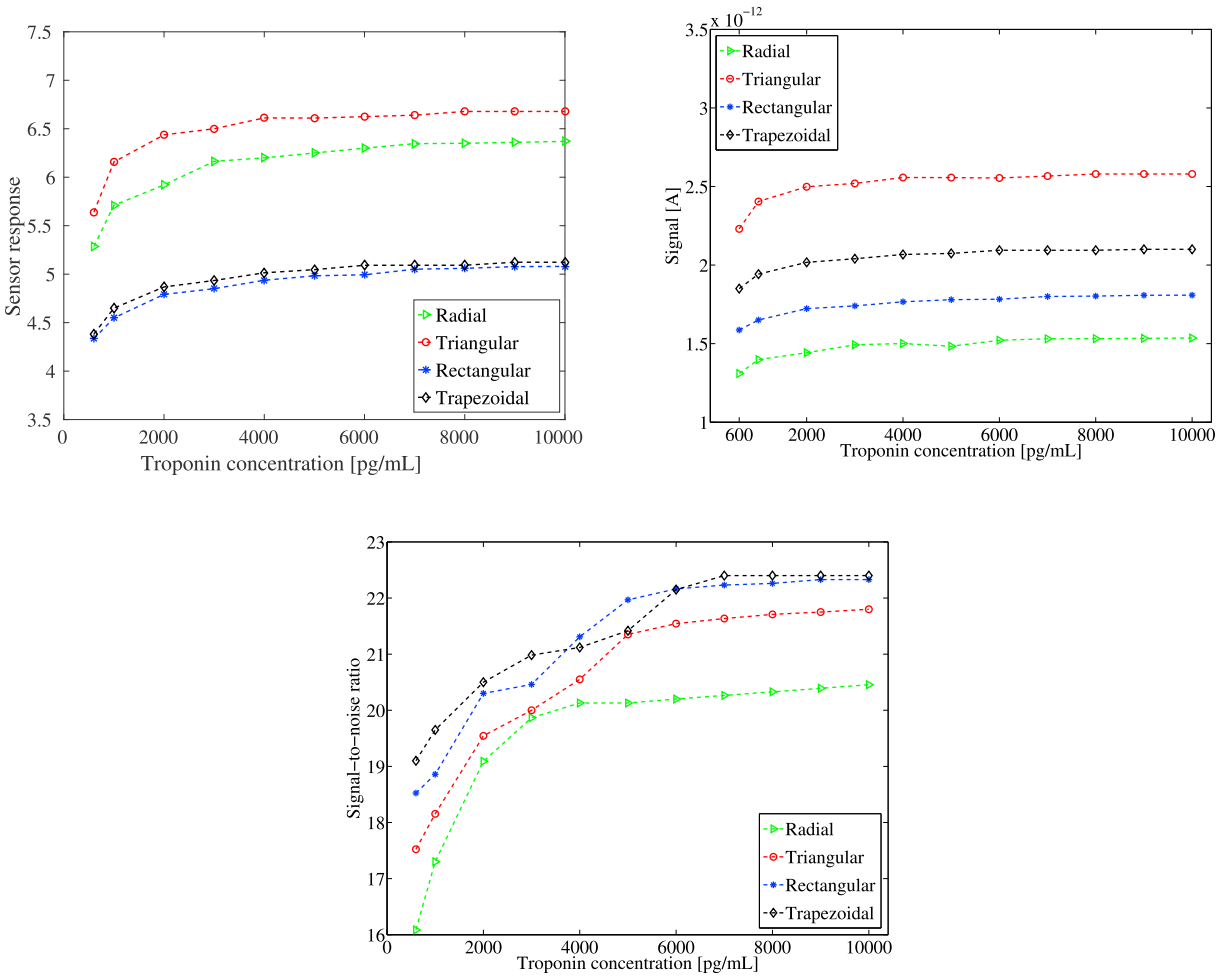

Fig. 10. Sensitivity (top left), signal (top right), and SNR (bottom) as a function of troponin concentration varying from 500 pg/mL and 10 ng/mL for different nanowires cross sections. The sensor is 1000 nm wide and the bulk oxide is 300 nm thick. Each sensor has four parallel 5000 nm long nanowires, a cross-sectional area of 2500 nm^2, a doping concentration of 10^{17} cm^{-3}, and they are protected by a 5 nm thick silicon oxide layer.

10^{16} cm^{-3} to 4×10^{17} cm^{-3}, the change in the sensitivity is negligible. This fact indicates that this interval is a suitable range for the sensor. For higher doping concentrations, the sensitivity decreases considerably for all devices, since the nanowires are mostly affected by the doping and the effect of charged molecules on the signal decreases. As is seen, the doping concentration affects noticeably the sensitivity only at high doping levels (decreasing it). Thus, lower concentrations (i.e., less than 4×10^{17} cm^{-3}) are more suitable for achieving a higher sensor response. This fact is shown by the signal curve, where the increment is approximately five orders of magnitude. Regarding the noise, it decreases when the doping concentration increases as already indicated since the nanowires are not affected as much by the fluctuation of the molecules. This effect causes a dramatic increase in SNR.

Although absolute cTn elevations are seen in multiple chronic cardiac and noncardiac conditions, a rise in serial cTn levels strongly support an acutely evolving cardiac injury such as most commonly, acute myocardial infarction. As aforementioned, larger sensors are used for higher concentrations. As Fig. 8 shows, the triangular nanowire is again the most sensitive device and the rectangular and trapezoidal show the same performance. Also, higher concentration increases the sensitivity of the device. The same holds for the signal, which doubles from 50 pg/ml to 500 pg/ml. The SNR increases with higher concentrations, while the devices show small fluctuations. The peak SNR is reached at 500 pg/ml.

This simulation capability also makes it possible to study the arrangement of the nanowires. More precisely, the distance between the nanowires is an important parameter for increasing the sensitivity. Fig. 1 depicts the arrangement of the nanowires indicating the center-to-center distance d between the nanowires and the distance d_1 between a nanowire and the boundary. Fig. 9 shows the sensitivity of sensors with two nanowires whose distance d varies between 150 nm and 850 nm. The sensor width $d+2d_1$ is 1000 nm. For larger distances, i.e., $d>750$ nm, the effect of charged molecules on the transducers decreases since the nanowires are closer to the boundaries. For distances less than 250 nm, the competition between the transducers to bind the target molecules gives rise to a decrease in the sensitivity. The simulations show that the maximum sensitivity for all transducer shapes is obtained for a center-to-center distance of 350 nm (symmetric arrangement).

In high-risk myocardial infarction patients, the cTn concentration reaches its peak approximately after six hours. In this time interval, the concentration rises sharply. For the concentration range from 500 pg/mL to 10 ng/mL, we use a sensor with four parallel nanowires. The results are shown in Fig. 10. Similar to the previous ranges, the triangular nanowire performs more efficiently. Due to the noticeably higher number of target molecules, the sensitivity is considerably higher than in the first range. Most of the receptors are bound to target molecules. This fact is more pronounced in the SNR since the simultaneously high **PT**-concentration (close to C_P) and small variance decrease the noise significantly.

4. Conclusions

In this work, we developed a comprehensive simulation capability of nanowire field-effect sensors based on a system of stochastic transport

equations and a stochastic reaction model for the association/dissociation process of target and probe molecules.

The troponin sensitive sensors developed here are important to shorten the heart-disease diagnostic time and to increase testing reliability. We considered the cardiac troponin concentration ranges of healthy and risky individuals and designed three sensors for three concentration ranges of clinical importance. Different influential physical parameters are studied in order to intensify the response of the sensor to different ranges of the protein and design the most sensitive device.

The shapes of the cross sections of the nanowires are often determined by the fabrication process. We simulated devices with four different cross sections of the same area. The triangular nanowires performed better than the other devices regarding sensor response and signal-to-noise ratio. Finally, the influence of the distances between nanowires arranged in arrays was studied. According to the simulations, a symmetric arrangement with proper distances between the nanowires is the best.

Conflict of interest

None declared.

Acknowledgment

The first and last authors acknowledge support by FWF (Austrian Science Fund) START project no. Y660 *PDE Models for Nanotechnology*. The authors also acknowledge the helpful comments by the anonymous reviewers.

References

[1] J.L. Anderson, C.D. Adams, E.M. Antman, C.R. Bridges, R.M. Califf, D.E. Casey, W.E. Chavey, F.M. Fesmire, J.S. Hochman, T.N. Levin, et al., ACC/AHA 2007 guidelines for the management of patients with unstable angina/non–ST-elevation myocardial infarction: a report of the American College of cardiology/American heart association task force on practice guidelines (writing committee to revise the 2002 guidelines for the management of patients with unstable angina/non–ST-elevation myocardial infarction) developed in collaboration with the American College of emergency physicians, the society for cardiovascular angiography and interventions, and the society of thoracic surgeons endorsed by the American association of cardiovascular and pulmonary rehabilitation and the society for Academic emergency medicine, J. Am. Coll. Cardiol. 50 (7) (2007) e1–e157.

[2] A. S. Go, D. Mozaffarian, V. L. Roger, E. J. Benjamin, J. D. Berry, M. J. Blaha, S. Dai, E. S. Ford, C. S. Fox, S. Franco, et al., Heart disease and stroke statistics-2014 update, Circulation 129(3).

[3] S. Allender, P. Scarborough, V. Peto, M. Rayner, J. Leal, R. Luengo-Fernandez, A. Gray, European Cardiovascular Disease Statistics.

[4] P. Stubbs, P.O. Collinson, Point-of-care testing: a cardiologist's view, Clin. Chim. Acta 311 (1) (2001) 57–61.

[5] K. Wang, R.W. Asinger, H.J. Marriott, ST-segment elevation in conditions other than acute myocardial infarction, N. Engl. J. Med. 349 (22) (2003) 2128–2135.

[6] L. Babuin, A.S. Jaffe, Troponin: the biomarker of choice for the detection of cardiac injury, Can. Med. Assoc. J. 173 (10) (2005) 1191–1202.

[7] T. Reichlin, W. Hochholzer, S. Bassetti, S. Steuer, C. Stelzig, S. Hartwiger, S. Biedert, N. Schaub, C. Buerge, M. Potocki, et al., Early diagnosis of myocardial infarction with sensitive cardiac troponin assays, N. Engl. J. Med. 361 (9) (2009) 858–867.

[8] M. Müller-Bardorff, K. Hallermayer, A. Schröder, C. Ebert, A. Borgya, W. Gerhardt, A. Remppis, J. Zehelein, H.A. Katus, Improved troponin T ELISA specific for cardiac troponin T isoform: assay development and analytical and clinical validation, Clin. Chem. 43 (3) (1997) 458–466.

[9] A. Bakker, R. Smits, F. Hagen, J. Gorgels, B. van Vlies, M. Koelemay, J. Tijssen, Failure of new biochemical markers to exclude acute myocardial infarction at admission, The Lancet 342 (8881) (1993) 1220–1222.

[10] R. De La Rica, M.M. Stevens, Plasmonic ELISA for the ultrasensitive detection of disease biomarkers with the naked eye, Nat. Nanotechnol. 7 (12) (2012) 821–824.

[11] B. Zhang, A.W. Morales, R. Peterson, L. Tang, J.Y. Ye, Label-free detection of cardiac troponin I with a photonic crystal biosensor, Biosens. Bioelectron. 58 (2014) 107–113.

[12] J.H. Chua, R.-E. Chee, A. Agarwal, S.M. Wong, G.-J. Zhang, Label-free electrical detection of cardiac biomarker with complementary metal-oxide semiconductor-compatible silicon nanowire sensor arrays, Anal. Chem. 81 (15) (2009) 6266–6271.

[13] W.-C. Law, K.-T. Yong, A. Baev, P.N. Prasad, Sensitivity improved surface plasmon resonance biosensor for cancer biomarker detection based on plasmonic enhancement, ACS Nano 5 (6) (2011) 4858–4864.

[14] S. Rana, A.K. Singla, A. Bajaj, S.G. Elci, O.R. Miranda, R. Mout, B. Yan, F.R. Jirik, V.M. Rotello, Array-based sensing of metastatic cells and tissues using nanoparticle-fluorescent protein conjugates, ACS Nano 6 (9) (2012) 8233.

[15] W. Shen, D. Tian, H. Cui, D. Yang, Z. Bian, Nanoparticle-based electrochemiluminescence immunosensor with enhanced sensitivity for cardiac troponin I using N-(aminobutyl)-N-(ethylisoluminol)-functionalized gold nanoparticles as labels, Biosens. Bioelectron. 27 (1) (2011) 18–24.

[16] K. Kim, C. Park, D. Kwon, D. Kim, M. Meyyappan, S. Jeon, J.-S. Lee, Silicon nanowire biosensors for detection of cardiac troponin I (ctni) with high sensitivity, Biosens. Bioelectron. 77 (2016) 695–701.

[17] K.-I. Chen, B.-R. Li, Y.-T. Chen, Silicon nanowire field-effect transistor-based biosensors for biomedical diagnosis and cellular recording investigation, Nano Today 6 (2) (2011) 131–154.

[18] L. Chang, J. Hu, F. Chen, Z. Chen, J. Shi, Z. Yang, Y. Li, L.J. Lee, Nanoscale bio-platforms for living cell interrogation: current status and future perspectives, Nanoscale 8 (6) (2016) 3181–3206.

[19] F. Patolsky, C.M. Lieber, Nanowire nanosensors, Mater. Today 8 (4) (2005) 20–28.

[20] T. Kuang, L. Chang, X. Peng, X. Hu, D. Gallego-Perez, Molecular beacon nano-sensors for probing living cancer cells, Trends Biotechnol..

[21] D. Gallego-Perez, L. Chang, J. Shi, J. Ma, S.-H. Kim, X. Zhao, V. Malkoc, X. Wang, M. Minata, K.J. Kwak, et al., On-chip clonal analysis of glioma-stem-cell motility and therapy resistance, Nano Lett. 16 (9) (2016) 5326–5332.

[22] J.-i. Hahm, C.M. Lieber, Direct ultrasensitive electrical detection of DNA and DNA sequence variations using nanowire nanosensors, Nano Lett. 4 (1) (2004) 51–54.

[23] G.-J. Zhang, J.H. Chua, R.-E. Chee, A. Agarwal, S.M. Wong, Label-free direct detection of MiRNAs with silicon nanowire biosensors, Biosens. Bioelectron. 24 (8) (2009) 2504–2508.

[24] E. Stern, J.F. Klemic, D.A. Routenberg, P.N. Wyrembak, D.B. Turner-Evans, A.D. Hamilton, D.A. LaVan, T.M. Fahmy, M.A. Reed, Label-free immunodetection with CMOS-compatible semiconducting nanowires, Nature 445 (7127) (2007) 519–522.

[25] A. Qureshi, Y. Gurbuz, J.H. Niazi, Biosensors for cardiac biomarkers detection: a review, Sens. Actuators B Chem. 171 (2012) 62–76.

[26] M.X. Li, L. Spyracopoulos, B.D. Sykes, Binding of cardiac Troponin-I147-163 induces a structural opening in human cardiac Troponin-C, Biochemistry 38 (26) (1999) 8289–8298.

[27] S. Takeda, A. Yamashita, K. Maeda, Y. Maeda, Structure of the core domain of human cardiac troponin in the Ca2+-saturated form, Nature 424 (6944) (2003) 35–41.

[28] A.H. Wu, The role of cardiac troponin in the recent redefinition of acute myocardial infarction, Clin. Lab. Sci. 17 (1) (2004) 50.

[29] J.L. McDonough, J.E. Van Eyk, Developing the next generation of cardiac markers: disease-induced modifications of troponin I, Prog. Cardiovasc. Dis. 47 (3) (2004) 207–216.

[30] A.V. Gomes, J.D. Potter, D. Szczesna-Cordary, The role of troponins in muscle contraction, IUBMB Life 54 (6) (2002) 323–333.

[31] S. Maynard, I. Menown, A. Adgey, Troponin T or Troponin I as Cardiac Markers in Ischaemic Heart Disease, 2000.

[32] I. Katrukha, Human cardiac troponin complex. structure and functions, Biochemistry 78 (13) (2013) 1447–1465 (Moscow).

[33] M.H. Ebell, D. Flewelling, C.A. Flynn, A systematic review of troponin T and I for diagnosing acute myocardial infarction, J. Fam. Pract. 49 (6) (2000), 550–550.

[34] V.S. Mahajan, P. Jarolim, How to interpret elevated cardiac troponin levels, Circulation 124 (21) (2011) 2350–2354.

[35] P. Venge, N. Johnston, B. Lindahl, S. James, Normal plasma levels of cardiac troponin I measured by the high-sensitivity cardiac troponin I access prototype assay and the impact on the diagnosis of myocardial ischemia, J. Am. Coll. Cardiol. 54 (13) (2009) 1165–1172.

[36] A. Saenger, R. Beyrau, S. Braun, R. Cooray, A. Dolci, H. Freidank, E. Giannitsis, S. Gustafson, B. Handy, H. Katus, et al., Multicenter analytical evaluation of a high-sensitivity troponin T assay, Clin. Chim. Acta 412 (9) (2011) 748–754.

[37] S. Sorgenfrei, C.-y. Chiu, R.L. Gonzalez Jr., Y.-J. Yu, P. Kim, C. Nuckolls, K.L. Shepard, Label-free single-molecule detection of dna-hybridization kinetics with a carbon nanotube field-effect transistor, Nat. Nanotechnol. 6 (2) (2011) 126–132.

[38] B. Lu, Y. Zhou, M. Holst, J. McCammon, Recent progress in numerical methods for the Poisson-Boltzmann equation in biophysical applications, Commun. Comput. Phys. 3 (5) (2008) 973–1009.

[39] A. Khodadadian, C. Heitzinger, Basis adaptation for the stochastic nonlinear Poisson–Boltzmann equation, J. Comput. Electron. 15 (4) (2016) 1393–1406.

[40] G. Tulzer, C. Heitzinger, Fluctuations due to association and dissociation processes at nanowire-biosensor surfaces and their optimal design, Nanotechnology 26 (2) (2014) 025502.

[41] G. Tulzer, C. Heitzinger, Brownian-motion based simulation of stochastic reaction–diffusion systems for affinity based sensors, Nanotechnology 27 (16) (2016) 165501.

[42] L. Taghizadeh, A. Khodadadian, C. Heitzinger, The optimal multilevel Monte-Carlo approximation of the stochastic drift–diffusion-Poisson system, Comput. Methods Appl. Mech. Eng. 318 (2017) 739–761.

[43] S. Baumgartner, C. Heitzinger, A. Vacic, M.A. Reed, Predictive simulations and optimization of nanowire field-effect PSA sensors including screening, Nanotechnology 24 (22) (2013), 225503/1–9.

[44] C. Heitzinger, C. Ringhofer, Multiscale modeling of fluctuations in stochastic elliptic PDE models of nanosensors, Commun. Math. Sci. 12 (3) (2014) 401–421.

[45] S. Baumgartner, C. Heitzinger, Existence and local uniqueness for 3D self-consistent multiscale models for field-effect sensors, Commun. Math. Sci. 10 (2) (2012) 693–716.

[46] C. Heitzinger, N.J. Mauser, C. Ringhofer, Multiscale modeling of planar and nanowire field-effect biosensors, SIAM J. Appl. Math. 70 (5) (2010) 1634–1654.

[47] S. Baumgartner, M. Vasicek, C. Heitzinger, Modeling and simulation of nanowire based field-effect biosensors, in: G. Korotcenkov (Ed.), Chemical Sensors: Simulation and Modeling, vol. 2, Momentum Press, 2012, pp. 447–469. Conductometric-Type Sensors.
[48] A. Bulyha, C. Heitzinger, An algorithm for three-dimensional Monte-Carlo simulation of charge distribution at biofunctionalized surfaces, Nanoscale 3 (4) (2011) 1608–1617.
[49] M.H. Olsson, C.R. Søndergaard, M. Rostkowski, J.H. Jensen, PROPKA3: consistent treatment of internal and surface residues in empirical pKa predictions, J. Chem. Theory Comput. 7 (2) (2011) 525–537.
[50] H. Li, A.D. Robertson, J.H. Jensen, Very fast empirical prediction and rationalization of protein pKa values, Proteins Struct. Funct. Bioinforma. 61 (4) (2005) 704–721.
[51] T.J. Dolinsky, P. Czodrowski, H. Li, J.E. Nielsen, J.H. Jensen, G. Klebe, N.A. Baker, PDB2PQR: expanding and upgrading automated preparation of biomolecular structures for molecular simulations, Nucleic Acids Res. 35 (suppl 2) (2007) W522–W525.
[52] A.W. Peterson, R.J. Heaton, R.M. Georgiadis, The effect of surface probe density on DNA hybridization, Nucleic Acids Res. 29 (24) (2001) 5163–5168.
[53] Y. Sandoval, F.S. Apple, The global need to define normality: the 99th percentile value of cardiac troponin, Clin. Chem. 60 (3) (2014) 455–462.
[54] X. Duan, Y. Li, N.K. Rajan, D.A. Routenberg, Y. Modis, M.A. Reed, Quantification of the affinities and kinetics of protein interactions using silicon nanowire biosensors, Nat. Nanotechnol. 7 (6) (2012) 401–407.
[55] M. Kuscu, O.B. Akan, On the physical design of molecular communication receiver based on nanoscale biosensors, IEEE Sens. J. 16 (8) (2016) 2228–2243.
[56] N. Elfström, R. Juhasz, I. Sychugov, T. Engfeldt, A. Eriksson Karlström, J. Linnros, Surface charge sensitivity of silicon nanowires: size dependence, Nano Lett. (Print) 7 (9) (2007) 2608–2612.
[57] S. Ramadan, K. Kwa, P. King, A. O'Neill, Reliable fabrication of sub-10 nm silicon nanowires by optical lithography, Nanotechnology 27 (42) (2016) 425302.
[58] N.F. Za'bah, K.S. Kwa, L. Bowen, B. Mendis, A. O'Neill, Top-down fabrication of single crystal silicon nanowire using optical lithography, J. Appl. Phys. 112 (2) (2012) 024309.